

The Diphoton q_T spectrum at $N^3LL'+NNLO$

TOBIAS NEUMANN¹

¹*Department of Physics, Brookhaven National Laboratory, Upton, New York 11973, USA,*

Abstract

We present a q_T -resummed calculation of diphoton production at order $N^3LL'+NNLO$. To reach the primed level of accuracy we have implemented the recently published three-loop $\mathcal{O}(\alpha_s^3)$ virtual corrections in the $q\bar{q}$ channel and the three-loop transverse momentum dependent beam functions and combined them with the existing infrastructure of CuTe-MCFM, a code performing resummation at order N^3LL . While the primed predictions are parametrically not more accurate, one typically observes from lower orders and other processes that they are the dominant effect of the next order. We include in both the $q\bar{q}$ and loop-induced gg channel the hard contributions consistently together at order α_s^3 and find that the resummed $q\bar{q}$ channel without matching stabilizes indeed. Due to large matching corrections and large contributions and uncertainties from the gg channel, the overall improvements are small though. We furthermore study the effect of hybrid-cone photon isolation and hard-scale choice on our fully matched results to describe the ATLAS 8 TeV data and find that the hybrid-cone isolation worsens agreement at small q_T compared to smooth-cone isolation.

The production of prompt isolated photon pairs at hadron colliders is a test of QCD with a clean experimental signature and constitutes as a background to the $h \rightarrow \gamma\gamma$ decay. Differential measurements at the LHC are available at 7 TeV, both by ATLAS and CMS [1–3], at 8 TeV by ATLAS [4], and very recently at 13 TeV also by ATLAS [5]. Further, many models of new physics predict resonant large mass diphoton decays for which events with diphoton invariant masses of up to ~ 2 TeV [6, 7] are used to constrain them.

Photons can either be produced directly or through the fragmentation of QCD partons. Photons produced through fragmentation require treatment of their singular collinear splitting. These singularities can be renormalized into non-perturbative fragmentation functions, but which are available only at NLO so far with large uncertainties [8, 9]. In higher-order calculations the collinear singularity is typically removed with a smooth-cone isolation prescription [10], which eliminates the collinear singularity, but does not prevent the usual cancellation of soft singularities. Quite some attention has been paid to the smooth-cone photon isolation procedure in recent years due to the uncertainty associated with the difference to experimental photon isolation [11–13].

NNLO calculations [14, 15] for diphoton production have shown large perturbative corrections with uncertainties that significantly underestimate the difference going from NLO to NNLO, estimated by using typical scale-

variation procedures. This is in part due to a new loop-induced gg channel entering at NNLO [15–18], but even true for just the Born-level induced $q\bar{q}$ channel. This has theorists led to deviate from the usual scale-variation prescription and suggest taking (half) the difference between NLO and NNLO as an estimate of the NNLO uncertainty [13]. This in turn mandates the calculation of higher-order predictions until uncertainties obtained from scale-variation stabilize. The inclusion of the recently published three-loop $q\bar{q} \rightarrow \gamma\gamma$ hard function [19] in the calculation presented in this paper contributes to these improvements.

Resummed predictions at small q_T are available at N^3LL [20] and at N^2LL [21], both matched to NNLO₀ fixed-order and have been computed previously at lower order matched to NLO₀ [22–25].¹ Recently, a matching to parton shower has been considered [26]. NLO electroweak effects have been studied in ref. [27], which are found to be less than one percent for the q_T distribution below 200 GeV, so they are not relevant for the results presented in this paper.

Uncertainties in the measured diphoton transverse momentum (q_T) and ϕ^* [28] distributions at 7 TeV and 8 TeV are about 10%. This is about the uncertainty

¹With the subscript 0 we denote that the order is with respect to the Born-level topology $\gamma\gamma$ and not with respect to $\gamma\gamma$ +jet, i.e. at large q_T . Latter would be denoted with a 1 subscript. Therefore $N^3LL+NNLO_0$ is equivalent to $N^3LL+NLO_1$. This is often ambiguous in the literature. In the following we will omit the 0 subscript.

estimated by scale variation from fixed-order NNLO ($\mathcal{O}(\alpha_s^2)$) and N³LL q_T -resummed calculations. While the uncertainties seem large, the differences between theory and measurement are found to be larger. Tensions start at $q_T \sim 15$ GeV and rise to differences of 30% between central values for q_T larger than 50 GeV [20].

Before moving on to a discussion about the photon isolation, we need to set up the relevant notation. The smooth-cone photon isolation prescription in this paper [10] restricts the transverse hadronic energy E_T^{had} around photons to be

$$E_T^{\text{had}} \leq E_T^{\text{iso}} \chi^{\text{smooth}}(r, R_s), \quad \forall r \leq R_s, \\ \chi^{\text{smooth}}(r, R_s) = \left(\frac{1 - \cos(r)}{1 - \cos(R_s)} \right)^n,$$

where E_T^{iso} is an isolation cone energy that can either be fixed or dependent on the photon transverse momentum, R_s is the isolation cone radius and n is a parameter. In this paper we also consider a simple hybrid-cone isolation that takes the smooth-cone isolation within an inner radius R_s and a fixed-cone prescription in the outer cone with radius R_o :

$$\chi^{\text{hybrid}}(r, R_s, R_o) = \begin{cases} \chi^{\text{smooth}}(r, R_s) & r \leq R_s \\ 1 & R_s < r < R_o \end{cases}.$$

Recently it has been argued that a bulk of the data-theory tensions are an artifact of two effects [11]. The first one is regarding the hard renormalization scale choice of $m_{\gamma\gamma}$ that has often been used for predictions. Since the diphoton pair is not produced resonantly, $m_{\gamma\gamma}$ is not the definite obvious choice for capturing the hard process kinematic scale. An alternative studied is to take the arithmetic mean of the photon transverse momenta $\langle q_T^\gamma \rangle$. The second effect is due to the photon isolation, which likely needs to be assigned larger uncertainties than previously thought. The suggestion is to use the hybrid-cone isolation, which allows for a better matching to the experimentally used fixed-cone prescription by adjusting the inner cone radius. An isolation uncertainty can then be obtained by varying the inner cone radius by some amount.

In ref. [11] it is further argued that isolation scheme and hard scale have compensating effects, at least for distributions sensitive to the photon separation $\Delta R_{\gamma\gamma}$ like the $m_{\gamma\gamma}$ distribution. The authors show that $\mu = m_{\gamma\gamma}$ plus

smooth-cone isolation and $\mu = \langle q_T^\gamma \rangle$ plus hybrid-cone isolation should go together, respectively, as there are compensating effects in the low and large mass region. Indeed they show that the agreement between data and theory is best for the combination of $\langle q_T^\gamma \rangle$ plus hybrid-cone isolation, but the experimental uncertainties in the large and small mass regions are also largest, leaving an unclear picture.

Every isolation prescription introduces an unphysical discontinuity due to the presence of step functions in the measurement function [29, 30]. At NNLO the discontinuity translates into a Sudakov singularity that has been studied in more detail in ref. [11]: In the case of the smooth-cone isolation the affected observable is not of experimental relevance. But the hybrid-cone isolation places this singularity directly into the $q_T^{\gamma\gamma}$ distribution around E_T^{iso} and its only cure is a sufficiently large experimental binning. Effectively, an overall better agreement in some distributions like $m_{\gamma\gamma}$ and at large q_T is traded for a worse agreement at small q_T , ϕ^* [28] or a_T [31] as well as for azimuthal photon separations $\Delta\Phi \sim \pi$. While these are all regions that need to be addressed by the resummation of large q_T/Q logarithms, we show that the discontinuity effects are amplified and that the agreement with data is *considerably* worsened: For the q_T distribution around E_T^{iso} and equivalently for Φ^* , the agreement of central values within a few percent is turned into disagreement of 50-60%, see our results in the following. Indeed in ref. [11] the authors anticipated problems with slicing subtractions. The q_T resummation (at leading power) in that sense acts like a slicing procedure, adding only Born-topology corrections on top of the fixed-order prediction that exhibits the Sudakov singularity. There is no compensating mechanism from the fixed-order expansion of the resummed result, resulting in the large unphysical matching corrections. The hybrid-cone isolation and natural scale choice also can unfortunately not help to address the large difference between α_s and α_s^2 results, but they raise valid concerns about previous assumptions.

Exactly this current situation makes a calculation of higher-order (α_s^3) effects necessary. They can hopefully unambiguously stabilize the perturbative series to allow for truncation uncertainties that can be trusted by finding overlapping bands between different orders in both the large and small q_T regions. A first step in that direction at large q_T is the very recent NNLO

calculation of $\gamma\gamma$ +jet [32]. This calculation predicts positive corrections at the order of 10% (without the loop-induced gg channel) below 100 GeV, which likely fills the currently seen gaps between NLO large- q_T predictions and data, see e.g. fig. 18 in ref. [20]. Also, since using the hybrid-cone isolation scheme with large- q_T NLO predictions leads to agreement with data within uncertainties, see ref. [11] and our plots in the following, it will be interesting to investigate how the additional 10% effects from a large- q_T NNLO prediction behave in the presence of this isolation scheme.

In the present study we demonstrate the effect of the α_s^3 hard functions, which are three-loop for the $q\bar{q}$ [19] channel and two-loop for the gg channel [17] (implemented in MCFM in refs. [15, 16]), and incorporate them with the recently published three-loop beam functions [33–35]. These ingredients are commonly referred to as “constant” pieces and including them to a higher order constitutes the primed accuracy, i.e. designated as $N^3LL' + NNLO_0$. The inclusion of the primed contributions is typically a dominant effect of the next order and also largely responsible for stabilization of truncation uncertainties. This can be seen by comparing for example resummed spectra at NLL' with N^2LL and N^2LL' with N^3LL . It is particularly true when matching corrections are small, such as in Drell-Yan production. This was recently observed in refs. [36, 37], and we also observe it in our N^3LL' implementation for Drell-Yan.

But while for Drell-Yan production q_T resummation works up to 40–50 GeV with almost negligible (1-2%) matching corrections [20, 38], the situation for photon processes is different due to the photon isolation [39]. With fiducial cuts the photon isolation prescription induces large linear power corrections [20]. Furthermore, the typical minimum $q_T^{\gamma,1}$ and $q_T^{\gamma,2}$ cuts on the two photons completely invalidate q_T resummation above $\sim q_T^{\gamma,1} + q_T^{\gamma,2}$ ($= 70$ GeV for the ATLAS 8 TeV study) and the matching corrections quickly grow towards that point. With these effects taken together, the matching corrections from fixed-order are 50-75% over the whole range of applicable q_T . This means that more than half of the cross-section at small q_T comes from the terms of the fixed-order prediction and are not described by the higher-order q_T -logarithms. Ideally one would like to resum the linear power corrections $\mathcal{O}(q_T/Q)$, but the isolation makes this difficult.

While several effects diminish stabilizing effects from

the inclusion of the three-loop $q\bar{q}$ hard function, the present calculation allows for a first inclusion of the three-loop virtual corrections in a physical calculation without the complication of a full N^3LO calculation, and therefore shows directly the impact of including these corrections. We also treat for the first time the $q\bar{q}$ and gg loop-induced α_s^3 hard functions fully consistently together in the resummation. Both channels have to be added separately together, of course, which means to reach the α_s^3 accuracy for the “constant” part, we add the N^3LL' resummed $q\bar{q}$ channel to the N^2LL resummed gg loop-induced channel.

Implementation. We extend the existing framework CuTe-MCFM [20] which implements N^3LL q_T resummation in the SCET formulation of refs. [40, 41] matched to fixed-order $NNLO_0$ [15, 16]. This framework achieves an accuracy of α_s^2 in improved perturbation theory at small and large q_T . To upgrade to N^3LL' accuracy we have implemented the one-, two- and three-loop \overline{MS} -renormalized virtual amplitudes from ref. [19] and restored the renormalization-scale dependence by solving the associated RGE [42] to order α_s^3 . For the numerical evaluation of harmonic polylogarithms up to weight six in the hard function we use the `hplog` library [43].² After that we find full agreement to machine precision with the existing one- and two-loop results in MCFM. The implemented \overline{MS} -renormalized amplitudes constitute the hard function. We also implemented the three-loop beam functions [33–35] and find that the double logarithmic $L_\perp \sim \log(x_T^2\mu^2)$ -dependence, where x_T is the fourier-conjugate of q_T , is as predicted by associated renormalization group equations [40]. For the resummation we employ an improved power counting $L_\perp \sim 1/\sqrt{\alpha_s}$ (relevant at small q_T), factor out the double-logarithmic L_\perp -dependence of the beam functions and exponentiate it through associated RGE [40]. In addition to the previously published version of CuTe-MCFM [20] we have also made the resummation scale uncertainties more robust by additionally varying the rapidity scale following ref. [44].

Results. Before showing differential results, we first discuss fiducial total cross-sections. At fixed order we

²We would like to thank Thomas Gehrmann for providing us with a version that computes the harmonic polylogarithms up to weight six.

can calculate these up to NNLO. For the q_T -resummed predictions we can simply integrate over q_T to obtain a total cross-section which includes higher-order logarithmic corrections. Ideally this is within the scale-uncertainties of the fixed-order result. Since the bulk of the cross-section comes from small q_T , the resummation can, in principle, improve the prediction and uncertainties. With N³LL' q_T resummation we can give a consistent prediction including both the $q\bar{q}$ - and gg -initiated hard functions at order α_s^3 .

For all results which follow, we implemented the parameter choices and cuts from the ATLAS 8 TeV study in ref. [45]. The selection cuts are $q_T^{\gamma,\text{hard}} > 40$ GeV, $q_T^{\gamma,\text{soft}} > 30$ GeV, $|\eta_\gamma| < 2.37$, omitting $1.37 < |\eta_\gamma| < 1.56$, $R_{\gamma\gamma} > 0.4$. The smooth-cone photon isolation criterion is used with $E_T^{\text{iso}} = 11$ GeV, $n = 1$ and $R_s = 0.4$. Throughout we use the NNPDF31_nnlo_as_0118 PDF set [46]. The measured fiducial cross-section is 16.8 ± 0.8 pb.

In table 1 we present the cross-sections for the $q\bar{q}$ and gg hard-function initiated processes at fixed-order and by integrating resummed cross-sections over q_T . Our resummation is matched to fixed-order predictions using a transition function as detailed in ref. [20]. The matching uncertainty from varying the transition function is about one percent at higher orders, i.e. small compared to the other uncertainties. We neglect matching corrections below 1 GeV, which has an effect smaller than the numerical precision quoted. For the fixed-order cross-sections the numbers in front of μ_R and μ_F denote a variation of the renormalization and factorization scale by a factor of 2 and 1/2, respectively. We only quote the maximum of upwards and downwards variation and take these as symmetric uncertainties. We also vary combinations, but their uncertainties are found to be smaller or similar. For the resummed predictions we correlate the renormalization scale μ_R with the hard scale and correlate the resummation scale with the factorization scale μ_F as in ref. [20]. To obtain robust uncertainties we additionally vary the rapidity-RGE scale, but find that these uncertainties are smaller than the resummation scale uncertainties for this process. In most studies all of these uncertainties are combined by taking the envelope. Here we just quote both numbers.

At NLO and NNLO we find indeed that the integrated resummed predictions agree within uncertainties with

Table 1: Cross-sections at 8 TeV for $q\bar{q}$ and gg hard-function initiated processes with $\mu_R = m_{\gamma\gamma}$ and smooth-cone isolation.

	$\sigma_{q\bar{q}}/\text{pb}$
NLO	$9.7 \pm 0.7(\mu_R) \pm 0.4(\mu_F)$
$\int \text{N}^2\text{LL} + \text{NLO}_0$	$8.9 \pm 1.1(\mu_R) \pm 0.9(\mu_F)$
NNLO	$12.8 \pm 1.8(\mu_R) \pm 0.2(\mu_F)$
$\int \text{N}^3\text{LL} + \text{NNLO}_0$	$12.7 \pm 0.9(\mu_R) \pm 0.4(\mu_F)$
$\int \text{N}^3\text{LL}' + \text{NNLO}_0$	$12.8 \pm 0.9(\mu_R) \pm 0.4(\mu_F)$
	σ_{gg}/pb
LO	$1.0 \pm 0.2(\mu_R) \pm 0.0(\mu_F)$
NLO	$2.0 \pm 0.4(\mu_R) \pm 0.1(\mu_F)$
$\int \text{N}^2\text{LL} + \text{NLO}_0$	$1.0 \pm 0.5(\mu_R) \pm 0.1(\mu_F)$

the fixed-order result. At order α_s^2 (NNLO) the uncertainties of the resummed prediction are smaller. The primed prediction taking into account the α_s^3 constant terms ($\int \text{N}^3\text{LL}' + \text{NNLO}_0$) shows no significant changes compared to the α_s^2 prediction, neither in cross-section nor in uncertainties. To understand that underlying this is still a stabilization of the cross-section we have to look at the results differentially next. Taking together the $q\bar{q}$ and gg contributions, the prediction and measurement agree at best marginally within mutual uncertainties, which is a known issue.

As suggested in ref. [11] a more natural choice for the renormalization (hard) and factorization scale is to take the arithmetic average of the photon momenta $\mu_R = \langle q_T^\gamma \rangle$, so we consider this in addition to our standard choice of $\mu_R = \sqrt{(m_{\gamma\gamma})^2 + (q_T^{\gamma\gamma})^2}$. With this scale we present results at the highest orders in table 2. The cross-section increases noticeably by more than the size of the previous scale variation uncertainty, and is now in much better agreement with the measurement.

Additionally we compare with a hybrid-cone implementation where the inner smooth-cone radius is reduced to $R_s = 0.1$ and the outer radius is $R_o = 0.4$. The value of $R_s = 0.1$ has been suggested in ref. [11] to best match the ATLAS 8 TeV measurement and the fragmentation calculation. We therefore present results with both $\mu_R = \langle q_T^\gamma \rangle$ and an inner cone $R_s = 0.1$ in table 3. This time the central value already overshoots the measured

Table 2: Cross-sections at 8 TeV for $q\bar{q}$ and gg hard-function initiated processes with $\mu_R = \langle q_T^\gamma \rangle$ and smooth-cone isolation.

	$\sigma_{q\bar{q}}/\text{pb}$
$\int \text{N}^3\text{LL}' + \text{NNLO}_0$	$13.7 \pm 1.0(\mu_R) \pm 0.3(\mu_F)$
	σ_{gg}/pb
$\int \text{N}^2\text{LL} + \text{NLO}_0$	$1.8 \pm 1.0(\mu_R) \pm 0.2(\mu_F)$

Table 3: Cross-sections at 8 TeV for $q\bar{q}$ and gg hard-function initiated processes with $\mu_R = \langle q_T^\gamma \rangle$ and hybrid-cone isolation with inner cone angle $R_0 = 0.1$.

	$\sigma_{q\bar{q}}/\text{pb}$
$\int \text{N}^3\text{LL}' + \text{NNLO}_0$	$15.5 \pm 1.1(\mu_R) \pm 0.4(\mu_F)$
	σ_{gg}/pb
$\int \text{N}^2\text{LL} + \text{NLO}_0$	$1.9 \pm 1.0(\mu_R) \pm 0.2(\mu_F)$

central value, but is also within uncertainties. To visualize the results of tables 1 to 3 and directly compare with the measurement, we show selected combinations in fig. 1, where the $q\bar{q}$ and loop-induced gg channel are combined consistently at the same order of α_s .

The resummed q_T spectrum without matching. Differentially, we first discuss the resummed q_T distributions without matching. We also focus only on the $q\bar{q}$ channel first, where we now include the α_s^3 hard function at $\text{N}^3\text{LL}'$. This is shown in fig. 2.

The bottom plot shows the ratio to the highest-order prediction $\text{N}^3\text{LL}'$, while the upper plot shows the absolute distributions. The N^2LL result takes into account just the α_s hard function, while $\text{N}^2\text{LL}'$ and N^3LL take into account the α_s^2 hard function but differ in the order of RGE solution that resums the large logarithms. Only N^3LL is fully consistent to order α_s^2 in improved perturbation theory.

The displayed uncertainties are obtained from the envelope of a variation of hard scale, resummation scale and rapidity scale. Since we use the envelope, the largest un-

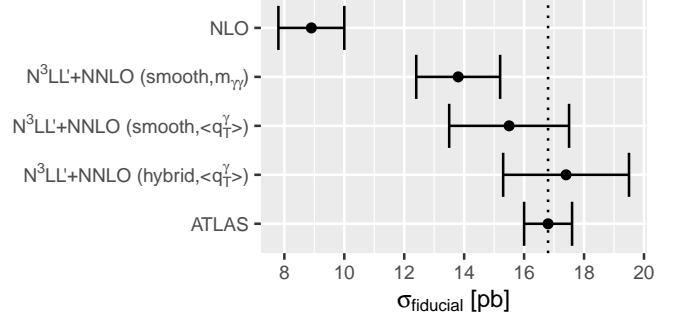


Figure 1: Comparison of selected fiducial cross-sections from tables 1 to 3 with the 8 TeV ATLAS measurement. Here both the $q\bar{q}$ and loop-induced gg channel contributions are added together consistently.

certainty determines the band, which in our case is from the resummation scale. Below 4 GeV the uncertainties turn constant for the following reason. In any resummation formalism a cutoff at small q_T is necessary since, for example, otherwise α_s would be evaluated at scales where non-perturbative effects become significant, i.e. where α_s becomes large. We choose to set a minimum scale of 2 GeV, which consequently leads to frozen out uncertainties below 4 GeV when a downwards scale variation becomes ineffective. Without such a cutoff the uncertainties would become arbitrarily large and would not represent realistic perturbative uncertainties, in addition to numerical problems.

Overall the uncertainties decrease going from N^2LL to higher orders. At the smallest q_T the uncertainties for N^2LL are about 20% and reduce to 12% going towards N^3LL , but change little between N^3LL and $\text{N}^3\text{LL}'$, likely an effect due to the same order in RGE running. For larger q_T we compare N^2LL , $\text{N}^2\text{LL}'$ and N^3LL and find that the primed accuracy, taking into account the higher-order hard and beam functions but solving the RGEs to a lower order, is responsible for the bulk of corrections. This is reflected by the good agreement between the orange and blue lines. Consequently one expects that the inclusion of the α_s^3 hard and beam functions is responsible for the bulk of corrections within a consistent N^4LL calculation. Indeed the highest-order prediction $\text{N}^3\text{LL}'$ is between both lower order predictions and noticeably decreases uncertainties above 10 GeV.

These findings indicate a stabilization of the $q\bar{q}$ channel,

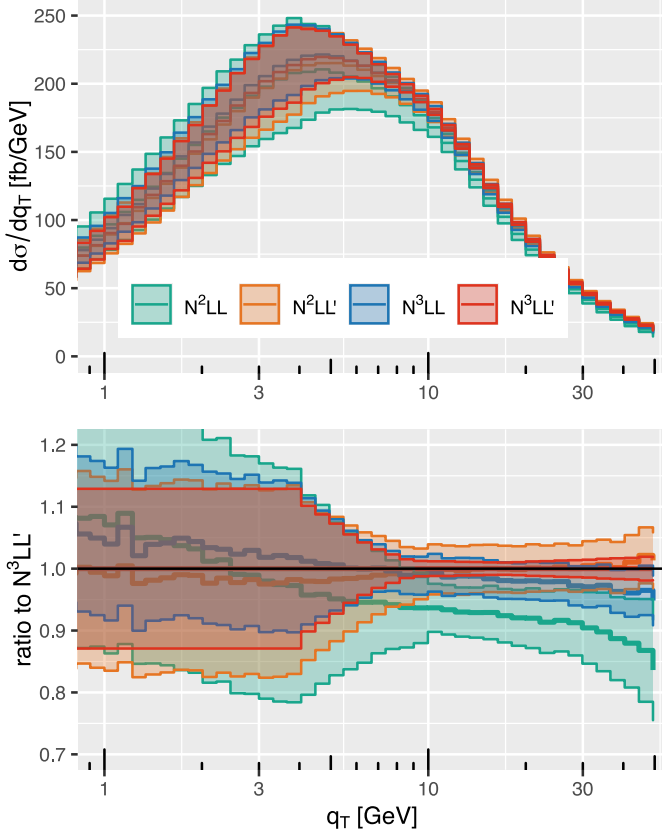


Figure 2: Resummed q_T spectrum without transition function nor matching for $q\bar{q}$ -initiated hard function at different orders. Top plot: absolute distributions. Bottom plot: ratio to N^3LL' .

but at order α_s^2 the loop-induced $gg \rightarrow \gamma\gamma$ channel enters that is enhanced due to the large gluon luminosity at the LHC at small momentum fractions. In fig. 3 we include this channel at the respective orders, i.e. the α_s^2 hard function at N^3LL and the α_s^3 hard function at N^3LL' . The gg channel is a substantial contribution with *huge* uncertainties. At low q_T the uncertainties are still at the order of 10%. Towards larger q_T the gg channel contributes “only” half of the cross-section, but the uncertainties are so large that the $q\bar{q}$ channel uncertainties of 1–2% seen in fig. 2 blow up to 10% in the sum of both channels. This is not unexpected since the gg channel, despite being of order α_s^3 is only NLO, respectively N^2LL +NLO accurate. To increase the precision in the intermediate low q_T region of about 10–50 GeV where resummation remains relevant, three-loop α_s^4 corrections to the gg channel will therefore be

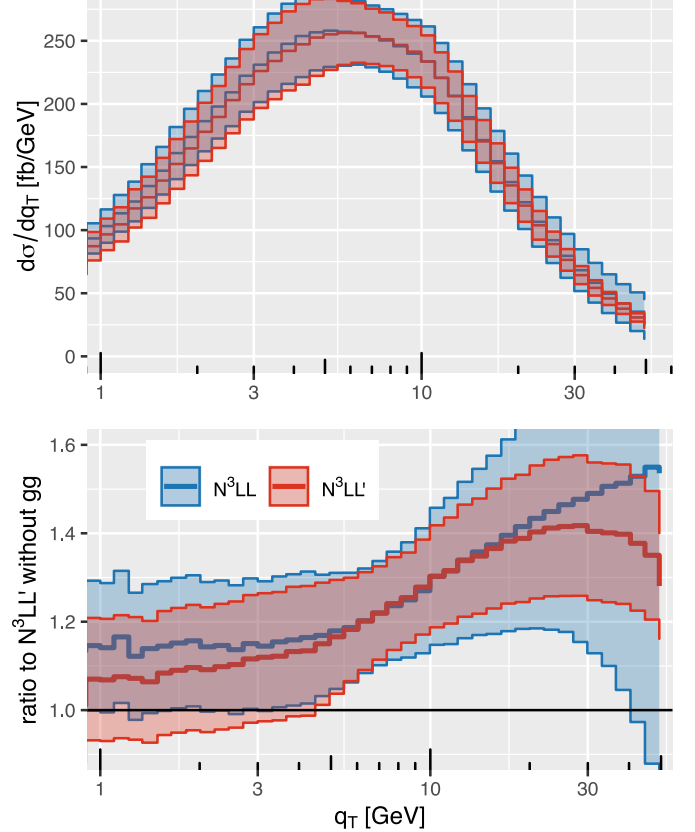


Figure 3: Resummed q_T spectrum without transition function nor matching including both $q\bar{q}$ and gg channels. Top plot: absolute distributions. Bottom plot: ratio to N^3LL' without gg channel.

important.

Fully matched results. We now move on to show fully matched results and directly compare with the 8 TeV ATLAS measurement. Our transition function is a function of $x = q_T^2/m_{\gamma\gamma}^2$ with a parameter x^{\max} that determines the transition region, see ref. [20] for a detailed description. For the following plots we use $x^{\max} = 0.1$ that performs the transition mostly in the region between 20 and 50 GeV. Since $m_{\gamma\gamma}$ is not sharply peaked as in resonant boson production, there is a tail of larger $m_{\gamma\gamma}$, for which the transition is later, such that we need to choose x^{\max} relatively small to prevent reaching ~ 70 GeV where the resummation breaks down due to the given photon cuts. We estimate the matching uncertainty by varying the transition function to use

$x^{\max} = 0.2$. This shifts the transition to be between 30 and 70 GeV. The resulting difference is small compared to our presented uncertainty bands obtained by scale variation.

So far the stabilization of the resummed $q\bar{q}$ channel has been somewhat overshadowed by large gg channel uncertainties. We now show the fully matched result in fig. 4 with ATLAS binning. The matching corrections at α_s^2 for diphoton production are sizable about 50%, as can also be seen by comparing with fig. 3. The top plot shows the absolute predictions for $N^3LL+NNLO$ and $N^3LL'+NNLO$, while the lower plot shows the ratio to the higher-order prediction without the gg channel. The higher-order corrections from the $q\bar{q}$ channel are small as we have seen, but the α_s^3 corrections on the gg channel have a noticeable impact (at large q_T we include the α_s^3 matching corrections in this channel). In both cases the uncertainties are large and transition into fixed-order uncertainties of about 15% at large q_T . Overall both predictions show uniform uncertainties of 10-15%.

To decrease uncertainties noticeably we will first have to include α_s^3 matching-corrections also in the $q\bar{q}$ channel, which at low q_T make up about 50% of the cross-section. Second, the gg channel has to be included at α_s^4 since it contributes an equal amount to the total uncertainty.

We finally show the fully matched results in comparison with the ATLAS measurement in fig. 5. The top plot shows the ratio of the ATLAS measurement to our highest-order prediction as in fig. 4. We furthermore included a prediction where the hard scale is chosen as $\langle q_T^{\gamma} \rangle$ as suggested in ref. [11]. This more natural scale choice closes the uncertainty gap, and prediction and measurement have now overlapping uncertainty bands.

The bottom plot includes additionally a prediction with the hybrid-cone isolation using an inner-cone radius of $R_s = 0.1$, where the previous agreement at small q_T is now destroyed. As already shown in ref. [11], the fixed-order predictions with hybrid-cone isolation at small Φ^* are worse than the smooth-cone isolation results.³ The authors suggest that “The regions where agreement

³To our surprise they do not find this to be true for small q_T , even though the region of small q_T and Φ^* should map onto each other.

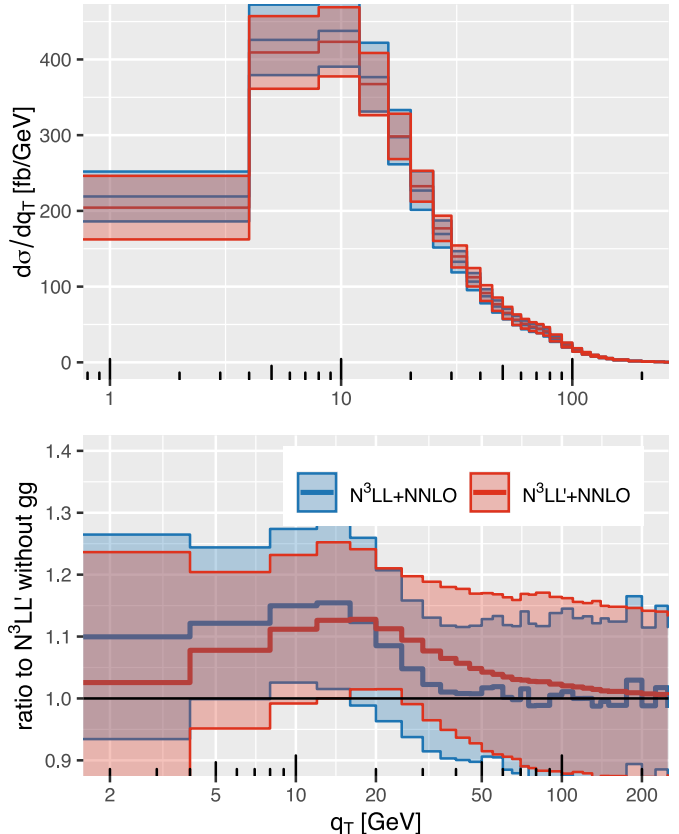


Figure 4: Fully matched q_T spectra at $N^3LL+NNLO$ and $N^3LL'+NNLO$. Top plot: absolute distributions. Bottom plot: ratio to $N^3LL'+NNLO$ without gg channel.

is notably worse are those in the neighborhood of the Sudakov singularities [...], and hence where poor agreement is expected in the absence of resummation”. While this is true, the distortion due to the hybrid-cone isolation of the q_T distribution cannot be cured by the present q_T resummation, but would require some other resummation.

In the limit of inner cone approaching outer cone $R_s \rightarrow R_o$ the smooth-cone isolation is restored by definition. In this limit the resummed results agree well with the data. For successively smaller R_s the cross-section coming from fixed-cone isolation grows. Since it is always larger than the contribution from smooth-cone isolation, the agreement at large q_T also grows. But the increase in cross-section is unfortunately not just at large q_T : the smaller R_s is taken, the larger the ridge at $q_T = E_T^{\text{iso}}$ becomes (see e.g. fig. 8 in ref. [11]). This ridge effect can be smoothed out to some extent by choosing a

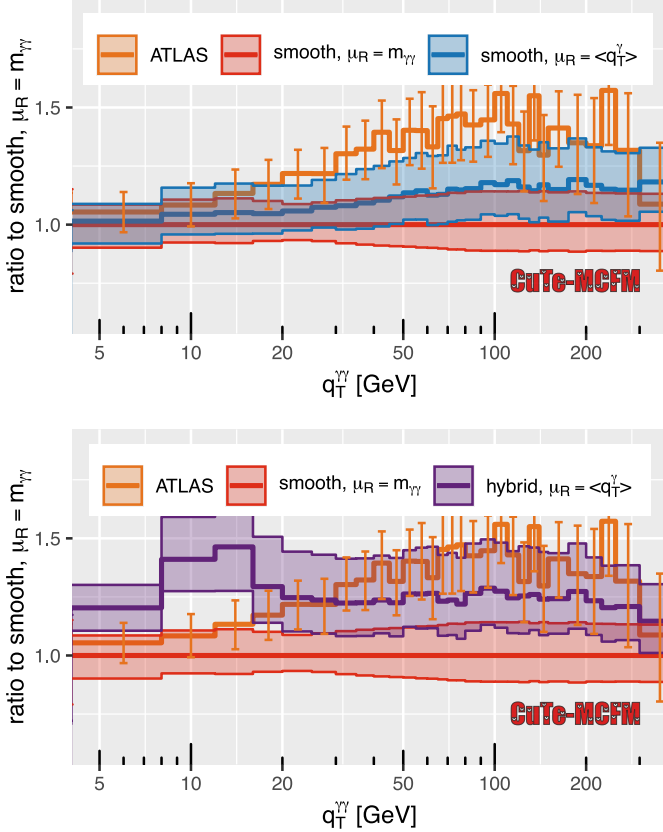


Figure 5: Fully matched q_T spectra at $N^3LL'+NNLO$ in comparison with the ATLAS measurement. Top plot: Ratio to N^3LL' with smooth-cone isolation and $\mu_R = m_{\gamma\gamma}$ in comparison with data and $\mu_R = \langle q_T^\gamma \rangle$. Bottom plot: Similar, but in comparison with prediction using hybrid-cone isolation and $\mu_R = \langle q_T^\gamma \rangle$.

non-constant E_T^{iso} , but would also have to be matched by the experimental definition.

We conclude that with present theory frameworks the hybrid-cone isolation is not the answer to a better modeling of photon isolation, especially with increased experimental precision. Distortion effects in the q_T distribution due to hybrid-cone isolation are only exacerbated by the q_T resummation. Better agreement at large q_T is traded with drastic disagreement at small q_T , where excellent agreement with resummation is achieved using the smooth-cone isolation. While it is possible to shift the Sudakov singularity in phase space, we believe that at this point the program for fragmentation functions will have to be revived.

For practical comparison with data, the lesson to be learned is likely to just take the more natural scale choice $\mu_R = \langle q_T^\gamma \rangle$, which brings theory and data into better agreement, and include the NNLO $\gamma\gamma$ +jet corrections [32]. We also show comparison plots for the Φ^* distribution in fig. 6 with similar observations at small Φ^* , since it is directly correlated to small q_T , but with worse agreement at large Φ^* .

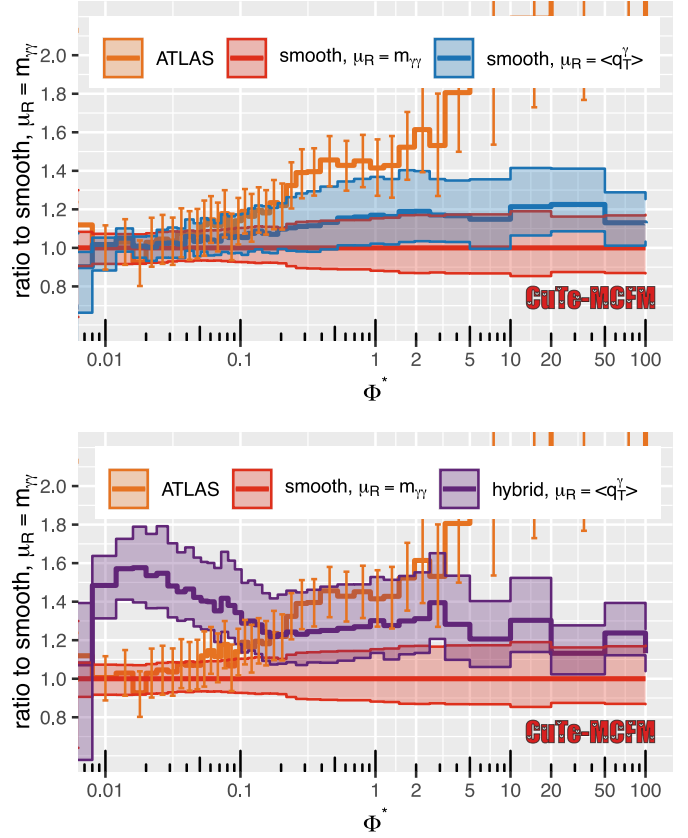


Figure 6: Fully matched ϕ^* spectra at $N^3LL'+NNLO$ in comparison with the ATLAS measurement. Top plot: Ratio to N^3LL' with smooth-cone isolation and $\mu_R = m_{\gamma\gamma}$ in comparison with data and $\mu_R = \langle q_T^\gamma \rangle$. Bottom plot: Similar, but in comparison with prediction using hybrid-cone isolation and $\mu_R = \langle q_T^\gamma \rangle$.

Conclusions. We have upgraded previous diphoton predictions at small q_T accurate at the level of α_s^2 in improved perturbation theory to include the α_s^3 “constant” pieces. These include the recently published three-loop $q\bar{q}$ hard function [19] and the previously implemented two-loop gg hard function [17] together with the three-

loop transverse momentum dependent beam functions [33–35]. This constitutes an overall primed resummation accuracy of $N^3LL' + NNLO_0$. The resummation itself of the $q\bar{q}$ channel is noticeably stabilized with remaining uncertainties of a few percent at intermediate q_T between 10 GeV and 50 GeV. But this is diminished by the large uncertainties from the gg channel at α_s^3 and large matching corrections.

With that, we have eliminated the $\alpha_s^3 q\bar{q}$ hard part as a source of uncertainty, and can limit the remaining sources of higher-order uncertainty and contributions for the q_T distribution: The dominating uncertainties will be reduced by a matching to $\gamma\gamma$ +jet at NNLO, which has 10% effects due to the $q\bar{q}$ channel below 100 GeV [32], and by α_s^4 corrections to the gg loop-induced channel, which are mostly relevant for $q_T \lesssim 200$ GeV.

We have shown that the more natural hard and renormalization scale $\langle q_T^2 \rangle$ with smooth-cone isolation alone restores agreement with data for the q_T distribution and for not too large Φ^* . On the other hand the hybrid-cone isolation (with fixed E_T^{iso}) introduces a discontinuity in the q_T distribution that destroys the otherwise agreement with data at small q_T . This is because the isolation is only a power-suppressed effect in the resummation. The leading-power resummation acts at the level of the Born-topology without isolation effects and cannot compensate the Sudakov singularity induced by the hybrid-cone isolation at fixed-order [11]. The upgrades presented in this paper will be included in the upcoming release of CuTe-MCFM⁴.

In the future we plan to match with a $\gamma\gamma$ +jet calculation at NNLO to take into account the full α_s^3 matching corrections at as small q_T as possible. If small enough q_T can be achieved numerically, one could also extract fixed-order N^3LO cross-sections using q_T slicing, but this will require cutoffs lower than 1 GeV, which is already numerically quite expensive at NNLO [15]. The implementation of the three-loop beam functions also facilitates an implementation of a single-boson $N^3LL' + NNLO_1$ implementation in MCFM.

Acknowledgments. We would like to thank Thomas Becher, John Campbell and Sally Dawson for useful discussion and comments on this manuscript. Tobias

Neumann is supported by the United States Department of Energy under Grant Contract DE-SC0012704. This work was supported by resources provided by the Scientific Data and Computing Center (SDCC), a component of the Computational Science Initiative (CSI) at Brookhaven National Laboratory (BNL).

References

- [1] CMS collaboration, *Measurement of differential cross sections for the production of a pair of isolated photons in pp collisions at $\sqrt{s} = 7$ TeV*, *Eur. Phys. J. C* **74** (2014) 3129 [1405.7225].
- [2] ATLAS collaboration, *Measurement of the isolated di-photon cross-section in pp collisions at $\sqrt{s} = 7$ TeV with the ATLAS detector*, *Phys. Rev. D* **85** (2012) 012003 [1107.0581].
- [3] ATLAS collaboration, *Measurement of isolated-photon pair production in pp collisions at $\sqrt{s} = 7$ TeV with the ATLAS detector*, *JHEP* **01** (2013) 086 [1211.1913].
- [4] ATLAS collaboration, *Measurements of integrated and differential cross sections for isolated photon pair production in pp collisions at $\sqrt{s} = 8$ TeV with the ATLAS detector*, *Phys. Rev. D* **95** (2017) 112005 [1704.03839].
- [5] ATLAS collaboration, *Measurement of the production cross section of pairs of isolated photons in pp collisions at 13 TeV with the ATLAS detector*, 2107.09330.
- [6] ATLAS collaboration, *Search for new phenomena in high-mass diphoton final states using 37 fb^{-1} of proton-proton collisions collected at $\sqrt{s} = 13$ TeV with the ATLAS detector*, *Phys. Lett. B* **775** (2017) 105 [1707.04147].
- [7] CMS collaboration, *Search for physics beyond the standard model in high-mass diphoton events from proton-proton collisions at $\sqrt{s} = 13$ TeV*, *Phys. Rev. D* **98** (2018) 092001 [1809.00327].
- [8] T. Kaufmann, A. Mukherjee and W. Vogelsang, *Recent developments on parton-to-photon fragmentation functions*, *CERN Proc.* **1** (2018) 211 [1708.06683].

⁴CuTe-MCFM is available at <https://mcfm.fnal.gov/>.

- [9] A. Gehrmann-De Ridder and E. W. N. Glover, *A Complete $\mathcal{O}(\alpha_s)$ calculation of the photon + 1 jet rate in $e^+ e^-$ annihilation*, *Nucl. Phys. B* **517** (1998) 269 [[hep-ph/9707224](#)].
- [10] S. Frixione, *Isolated photons in perturbative QCD*, *Phys. Lett. B* **429** (1998) 369 [[hep-ph/9801442](#)].
- [11] T. Gehrmann, N. Glover, A. Huss and J. Whitehead, *Scale and isolation sensitivity of diphoton distributions at the LHC*, *JHEP* **01** (2021) 108 [[2009.11310](#)].
- [12] X. Chen, T. Gehrmann, N. Glover, M. Höfer and A. Huss, *Isolated photon and photon+jet production at NNLO QCD accuracy*, *JHEP* **04** (2020) 166 [[1904.01044](#)].
- [13] S. Catani, L. Cieri, D. de Florian, G. Ferrera and M. Grazzini, *Diphoton production at the LHC: a QCD study up to NNLO*, *JHEP* **04** (2018) 142 [[1802.02095](#)].
- [14] S. Catani, L. Cieri, D. de Florian, G. Ferrera and M. Grazzini, *Diphoton production at hadron colliders: a fully-differential QCD calculation at NNLO*, *Phys. Rev. Lett.* **108** (2012) 072001 [[1110.2375](#)].
- [15] J. M. Campbell, R. K. Ellis, Y. Li and C. Williams, *Predictions for diphoton production at the LHC through NNLO in QCD*, *JHEP* **07** (2016) 148 [[1603.02663](#)].
- [16] J. M. Campbell, R. K. Ellis and C. Williams, *Vector boson pair production at the LHC*, *JHEP* **07** (2011) 018 [[1105.0020](#)].
- [17] Z. Bern, A. De Freitas and L. J. Dixon, *Two loop amplitudes for gluon fusion into two photons*, *JHEP* **09** (2001) 037 [[hep-ph/0109078](#)].
- [18] E. W. N. Glover and M. E. Tejeda-Yeomans, *Two loop QCD helicity amplitudes for massless quark massless gauge boson scattering*, *JHEP* **06** (2003) 033 [[hep-ph/0304169](#)].
- [19] F. Caola, A. Von Manteuffel and L. Tancredi, *Diphoton Amplitudes in Three-Loop Quantum Chromodynamics*, *Phys. Rev. Lett.* **126** (2021) 112004 [[2011.13946](#)].
- [20] T. Becher and T. Neumann, *Fiducial $q\bar{q}$ resummation of color-singlet processes at $N^3LL+NNLO$* , *JHEP* **03** (2021) 199 [[2009.11437](#)].
- [21] L. Cieri, F. Coradeschi and D. de Florian, *Diphoton production at hadron colliders: transverse-momentum resummation at next-to-next-to-leading logarithmic accuracy*, *JHEP* **06** (2015) 185 [[1505.03162](#)].
- [22] C. Balazs, E. L. Berger, P. M. Nadolsky and C. P. Yuan, *All-orders resummation for diphoton production at hadron colliders*, *Phys. Lett.* **B637** (2006) 235 [[hep-ph/0603037](#)].
- [23] C. Balazs, E. L. Berger, P. M. Nadolsky and C.-P. Yuan, *Calculation of prompt diphoton production cross-sections at Tevatron and LHC energies*, *Phys. Rev. D* **76** (2007) 013009 [[0704.0001](#)].
- [24] P. M. Nadolsky, C. Balazs, E. L. Berger and C. P. Yuan, *Gluon-gluon contributions to the production of continuum diphoton pairs at hadron colliders*, *Phys. Rev.* **D76** (2007) 013008 [[hep-ph/0702003](#)].
- [25] F. Coradeschi and T. Cridge, *reSolve — A transverse momentum resummation tool*, *Comput. Phys. Commun.* **238** (2019) 262 [[1711.02083](#)].
- [26] S. Alioli, A. Broggio, A. Gavardi, S. Kallweit, M. A. Lim, R. Nagar et al., *Precise predictions for photon pair production matched to parton showers in GENEVA*, *JHEP* **04** (2021) 041 [[2010.10498](#)].
- [27] M. Chiesa, N. Greiner, M. Schönherr and F. Tramontano, *Electroweak corrections to diphoton plus jets*, *JHEP* **10** (2017) 181 [[1706.09022](#)].
- [28] A. Banfi, S. Redford, M. Vesterinen, P. Waller and T. R. Wyatt, *Optimisation of variables for studying dilepton transverse momentum distributions at hadron colliders*, *Eur. Phys. J. C* **71** (2011) 1600 [[1009.1580](#)].
- [29] S. Catani and B. R. Webber, *Infrared safe but infinite: Soft gluon divergences inside the physical region*, *JHEP* **10** (1997) 005 [[hep-ph/9710333](#)].
- [30] T. Binoth, J. P. Guillet, E. Pilon and M. Werlen, *A Full next-to-leading order study of direct photon pair production in hadronic collisions*, *Eur. Phys. J. C* **16** (2000) 311 [[hep-ph/9911340](#)].

- [31] M. Vesterinen and T. R. Wyatt, *A Novel Technique for Studying the Z Boson Transverse Momentum Distribution at Hadron Colliders*, *Nucl. Instrum. Meth. A* **602** (2009) 432 [0807.4956].
- [32] H. A. Chawdhry, M. Czakon, A. Mitov and R. Poncelet, *NNLO QCD corrections to diphoton production with an additional jet at the LHC*, 2105.06940.
- [33] M.-x. Luo, T.-Z. Yang, H. X. Zhu and Y. J. Zhu, *Unpolarized quark and gluon TMD PDFs and FFs at N³LO*, *JHEP* **06** (2021) 115 [2012.03256].
- [34] M. A. Ebert, B. Mistlberger and G. Vita, *Transverse momentum dependent PDFs at N³LO*, *JHEP* **09** (2020) 146 [2006.05329].
- [35] M.-x. Luo, T.-Z. Yang, H. X. Zhu and Y. J. Zhu, *Quark Transverse Parton Distribution at the Next-to-Next-to-Next-to-Leading Order*, *Phys. Rev. Lett.* **124** (2020) 092001 [1912.05778].
- [36] E. Re, L. Rottoli and P. Torrielli, *Fiducial Higgs and Drell-Yan distributions at N³LL'+NNLO with RadISH*, 2104.07509.
- [37] W.-L. Ju and M. Schönherr, *The q_T and Δφ spectra in W and Z production at the LHC at N³LL'+N²LO*, 2106.11260.
- [38] M. A. Ebert, J. K. L. Michel, I. W. Stewart and F. J. Tackmann, *Drell-Yan q_T resummation of fiducial power corrections at N³LL*, *JHEP* **04** (2021) 102 [2006.11382].
- [39] M. A. Ebert and F. J. Tackmann, *Impact of isolation and fiducial cuts on q_T and N-jettiness subtractions*, *JHEP* **03** (2020) 158 [1911.08486].
- [40] T. Becher and M. Neubert, *Drell-Yan Production at Small q_T, Transverse Parton Distributions and the Collinear Anomaly*, *Eur. Phys. J.* **C71** (2011) 1665 [1007.4005].
- [41] T. Becher, M. Neubert and D. Wilhelm, *Electroweak Gauge-Boson Production at Small q_T: Infrared Safety from the Collinear Anomaly*, *JHEP* **02** (2012) 124 [1109.6027].
- [42] T. Becher and M. Neubert, *On the Structure of Infrared Singularities of Gauge-Theory Amplitudes*, *JHEP* **06** (2009) 081 [0903.1126].
- [43] T. Gehrmann and E. Remiddi, *Numerical evaluation of harmonic polylogarithms*, *Comput. Phys. Commun.* **141** (2001) 296 [hep-ph/0107173].
- [44] P. Jaiswal and T. Okui, *Reemergence of rapidity-scale uncertainty in soft-collinear effective theory*, *Phys. Rev. D* **92** (2015) 074035 [1506.07529].
- [45] ATLAS collaboration, *Measurements of integrated and differential cross sections for isolated photon pair production in pp collisions at √s = 8 TeV with the ATLAS detector*, *Phys. Rev.* **D95** (2017) 112005 [1704.03839].
- [46] NNPDF collaboration, *Parton distributions from high-precision collider data*, *Eur. Phys. J. C* **77** (2017) 663 [1706.00428].